Non-standard antineutrino interactions at Daya Bay

Rupert Leitner,[1, *] Michal Malinský,[2, †] Bedřich Roskovec,[1, ‡] and He Zhang[3, §]

[1]*Institute of Particle and Nuclear Physics,*

Faculty of Mathematics and Physics, Charles University in Prague,

V Holešovičkách 2, 180 00 Praha 8, Czech Republic

[2]*AHEP Group, Instituto de Física Corpuscular, C.S.I.C. – Universitat de València*

Edificio de Institutos de Paterna, Apartado 22085, E–46071 València, Spain

[3]*Max-Planck-Institut für Kernphysik,*

Postfach 103980, 69029 Heidelberg, Germany

Abstract

We study the prospects of pinning down the effects of non-standard antineutrino interactions in the source and in the detector at the Daya Bay neutrino facility. It is well known that if the non-standard interactions in the detection process are of the same type as those in the production, their net effect can be subsumed into a mere shift in the measured value of the leptonic mixing angle θ_{13}. Relaxing this assumption, the ratio of the antineutrino spectra measured by the Daya Bay far and near detectors is distorted in a characteristic way, and good fits based on the standard oscillation hypothesis are no longer viable. We show that, under certain conditions, three years of Daya Bay running can be sufficient to provide a clear hint of non-standard neutrino physics.

*Electronic address: Rupert.Leitner@cern.ch

†Electronic address: malinsky@ific.uv.es

‡Electronic address: roskovec@ipnp.troja.mff.cuni.cz

§Electronic address: he.zhang@mpi-hd.mpg.de

arXiv:1105.5580v1 [hep-ph] 27 May 2011

I. INTRODUCTION

The past and ongoing neutrino oscillation experiments provide a firm evidence that the neutrino flavor is changing throughout the neutrino propagation. Except for some recent signals reported by MINOS [1] and MiniBooNE [2] (and also previously by LSND [3]) the vast majority of the data is consistent with the hypothesis of neutrino flavor oscillations driven by a pair of mass-squared differences: $\Delta m_{31}^2 = 2.45 \pm 0.09 \times 10^{-3}$ eV^2 (or $\Delta m_{31}^2 = -(2.34_{-0.09}^{+0.10}) \times 10^{-3}$ eV^2 if an inverse neutrino mass hierarchy is realized), often called the atmospheric mass-squared difference, and the solar mass-squared difference $\Delta m_{21}^2 = 7.59_{-0.18}^{+0.20} \times 10^{-5}$ eV^2, together with a pair of the corresponding mixing angles: $\sin^2 \theta_{23} = 0.51 \pm 0.06$ (or $\sin^2 \theta_{23} = 0.52 \pm 0.06$ the inverse hierarchy case) and $\sin^2 \theta_{12} = 0.312_{-0.015}^{+0.017}$ [4]. This, however, requires at least two of the oscillating neutrinos to be massive.

By construction, neutrinos are massless in the Standard Model (SM). Thus, a lot of effort has been spent on devising SM extensions that could not only accommodate the unprecedented smallness of the light neutrino mass scale and all the peculiarities of the leptonic mixing pattern, but also provide specific new physics signals, thus admitting for a further experimental scrutiny. In some cases, such new physics effects could even be expected to be within the reach of near future experimental facilities. In this respect, the seesaw approach [5–12], in which the smallness of the absolute neutrino mass scale is usually linked to a very specific type of high energy dynamics, represents a particularly plausible model-building paradigm.

Each dynamical realization of the seesaw picture makes some kind of new physics effects appear, at least at a certain level. This, in turn, makes the neutrino sector an ideal probe to physics beyond the SM. For instance, the Majorana nature of the light neutrinos inherent to the seesaw framework provides characteristic lepton-number-violating signals at low energies like, e.g., the neutrinoless double beta decay, or, if kinematically accessible, same-sign di-lepton production at colliders, see, e.g., [13]. Similarly, besides neutrino oscillations, the flavor structure of the lepton sector can be tested in lepton-flavor-violating processes such as $\mu \to e\gamma$ or, for example, trilepton collider events, c.f., [14].

A full exploration of such new physics signals generally requires a very good knowledge of the leptonic flavor mixing angles governing the neutrino oscillation phenomena. In particular, the smallest mixing angle θ_{13}, which plays a central role in the leptonic CP violation,

is still to be determined (with a current 90% C.L. upper bound of $\sin^2 2\theta_{13} \lesssim 0.17$ reported by the CHOOZ collaboration [15]).

The Daya Bay neutrino oscillation experiment [16] is designed to perform a precision determination of θ_{13} with a potential to improve the CHOOZ limit by one order of magnitude. Its main virtue consists in a very good control over the systematics because of the unique set of eight identical detectors deployed at three different locations optimized for monitoring the antineutrino rates from the six reactors. A similar experimental setup is also adopted by the upcoming Double Chooz experiment [17] and RENO [18] experiments.

In combination with the large statistics due to the huge flux of antineutrinos produced in the nearby nuclear reactors, the unprecedented accuracy of this new generation of reactor experiments can make them sensitive to the new physics effects, at least at a certain level. For instance, if the new physics sector couples to hadrons and the relevant scale is not very high, one can expect non-standard interactions (NSI's) in the antineutrino production and detection processes as well as non-standard matter effects the antineutrinos experience throughout the propagation process. Similarly, new neutral fermions can mix with the three SM active neutrinos, which would result in an effective non-unitarity of the leptonic mixing matrix entering the relevant oscillations probabilities.

The NSI's in reactor neutrino experiments have been discussed previously in, e.g., [19, 20], especially when the production and detection processes (and the corresponding non-standard effects) are assumed to be just inverse of each other. In particular, it has been shown that in such a case the NSI effects can be subsumed into a mere shift in the measured value of the effective mixing angle θ_{13}.

In this work, we study the NSI's in reactor antineutrino experiments in a general case when the assumption that the source and at the detector processes including the non-standard effects are just inverse of each other is dropped. This, in turn, leads to a specific distortion in the ratio of the antineutrino spectra measured in the far and in the near detectors which can not be entirely transformed away by mere shifts in the relevant oscillation parameters, i.e., θ_{13} and Δm_{31}^2. We show that, under certain conditions, three years of Daya Bay running can be sufficient to provide a clear hint of non-standard neutrino physics.

The remainder of the manuscript is organized as follows: In Sec. II, we present the general formalism and derive the relevant antineutrino survival probability formulas used in the subsequent analysis. Two basic scenarios corresponding to qualitatively different shapes

of NSI's are specified in Sect. III, and a detailed analysis of the observability of such effects at Daya Bay is performed in Sect. IV. Finally, we conclude in Sect. V.

II.   NON-STANDARD INTERACTIONS IN REACTOR ANTINEUTRINO OSCILLATIONS

A.   Non-standard interactions in the antineutrino sources and detectors

In what follows, we adopt the standard SPD (source, propagation, and detector) approach [21] to consider the antineutrino oscillation process in a reactor antineutrino experiment. In the presence of NSI's, the antineutrino states produced in the source as well as those observed in the detector can be treated as superpositions of pure orthonormal flavor states

$$|\overline{\nu_\alpha^s}\rangle = |\overline{\nu_\alpha}\rangle + \sum_{\beta=e,\mu,\tau} \varepsilon_{\alpha\beta}^{s*}|\overline{\nu_\beta}\rangle \ , \qquad \langle\overline{\nu_\beta^d}| = \langle\overline{\nu_\beta}| + \sum_{\alpha=e,\mu,\tau} \varepsilon_{\alpha\beta}^{d*}\langle\overline{\nu_\alpha}| \ , \tag{1}$$

where the superscripts 's' and 'd' denote the source and the detector, respectively. Note that there is no need to include the appropriate normalization factors in expressions (1) because we are going to be interested only in ratios of the survival probabilities in the near and far detectors where such factors cancel.

The current experimental bounds on the NSI parameters mainly come from the lepton flavor violating decays $\ell_\alpha \to \ell_\beta\gamma$, the universality test of weak interactions and the invisible decay width of the Z-boson. Model-independent studies indicate that the upper limits on the NSI parameters $\varepsilon_{\alpha,\beta}^{s,d}$ are typically in the ballpark of 10^{-1} to 10^{-2}, see e.g. [22] and references therein.

Furthermore, let us also remark that the NSI parameter matrices ε^s and $\varepsilon^{d\dagger}$ need not be identical in view of the different conditions under which the antineutrino production and detection processes generally take place. This assumption, i.e., the non-equality of ε^s and $\varepsilon^{d\dagger}$, is, indeed, the key assumption adopted in this work. At the microscopic level, it can for instance correspond to non-standard antineutrino interactions with more than a single nucleon in the source or with a different kinematics of the production and detection processes. For further comments, an interested reader is deferred to Sect. III B.

B. Non-standard interactions in the antineutrino propagation

The propagation of antineutrino flavor eigenstates from the sources to the detectors is governed by the effective Hamiltonian

$$\hat{H} = H_0 + H_m + H_{\rm NSI} = \frac{1}{2E}U^*{\rm diag}(m_1^2, m_2^2, m_3^2)U^T - {\rm diag}(V_{\rm CC}, 0, 0) - V_{\rm CC}\varepsilon^{m*}, \quad (2)$$

where ε^m is a Hermitian matrix parametrizing the NSI's throughout the antineutrino propagation and $V_{\rm CC} = \sqrt{2}G_F N_e$ arises due to effects of the coherent forward scattering in matter (with N_e denoting the electron number density along the antineutrino trajectory). Barring the irrelevant Majorana phases, the vacuum leptonic mixing matrix U is conveniently parametrized by three mixing angles θ_{12}, θ_{23} and θ_{13} and one Dirac CP phase δ [23]

$$U = \begin{pmatrix} c_{12}c_{13} & s_{12}c_{13} & s_{13}e^{-i\delta} \\ -s_{12}c_{23} - c_{12}s_{23}s_{13}e^{i\delta} & c_{12}c_{23} - s_{12}s_{23}s_{13}e^{i\delta} & s_{23}c_{13} \\ s_{12}s_{23} - c_{12}c_{23}s_{13}e^{i\delta} & -c_{12}s_{23} - s_{12}c_{23}s_{13}e^{i\delta} & c_{23}c_{13} \end{pmatrix}, \quad (3)$$

with $c_{ij} \equiv \cos\theta_{ij}$ and $s_{ij} \equiv \sin\theta_{ij}$ (for $ij = 12$, 13 and 23). The full effective Hamiltonian (2) is diagonalized via a unitary transformation

$$\hat{H} = \frac{1}{2E}\hat{U}^*{\rm diag}\left(\hat{m}_1^2, \hat{m}_2^2, \hat{m}_3^2\right)\hat{U}^T, \quad (4)$$

where $\hat{m}_i$ ($i = 1, 2, 3$) denote the effective masses of neutrinos and $\hat{U}$ is the effective leptonic mixing matrix in matter.

The size of the matter effect driven by the $\sqrt{2}G_F N_e$ term amounts to around 1.1×10^{-7} eV^2/MeV for Earth crust with density of 2.8 g/cm^3. Even for the highest values of reactor antineutrino energies of around 10 MeV, this number is about 40 times smaller than the value of $\Delta m_{21}^2/(2E) = 3.8 \times 10^{-6}$ eV^2/MeV and about 1100 times smaller than $\Delta m_{32}^2/(2E) = 1.2 \times 10^{-4}$ eV^2/MeV. This indicates that Earth matter effects are very small and can be safely neglected. Hence, we take $\hat{H} \simeq H_0$ or, equivalently, set $V_{\rm CC} = 0$ in Eq. (2).

C. The antineutrino survival probability

With the NSI effects at play, the electron antineutrino survival probability amplitude $\mathcal{A}(\overline{\nu_e^s} \to \overline{\nu_e^d}; L) \equiv \mathcal{A}_{ee}(L)$ is given by

$$\mathcal{A}_{ee}(L) = \langle\overline{\nu_e^d}|e^{-iHL}|\overline{\nu_e^s}\rangle = (1 + \varepsilon^{d*})_{\rho e}A_{\gamma\rho}(1 + \varepsilon^{s*})_{e\gamma} = \left[A + \varepsilon^{s*}A + A\varepsilon^{d*} + \varepsilon^{s*}A\varepsilon^{d*}\right]_{ee}, \quad (5)$$

where L is the propagation distance and A is a coherent sum over the contributions of all the mass eigenstates ν_i

$$A_{\alpha\beta} = \sum_i U_{\alpha i} U_{\beta i}^* e^{-i\frac{m_i^2 L}{2E}} \ . \tag{6}$$

The antineutrino survival probability is then given by $P(\overline{\nu_e^s} \to \overline{\nu_e^d}) = |\mathcal{A}_{ee}(L)|^2$. For completeness, let us remark that a corresponding neutrino oscillation amplitude can be readily obtained from (5) with a substitution $(U^*, \varepsilon^*) \to (U, \varepsilon)$. It should also be stressed that only the first row of ε^s and the first column of ε^d are relevant to the ee-type transition amplitude. Namely, the NSI parameters ε^s and ε^d involved in reactor neutrino experiment contain at least one flavor index e.

Inserting formula (6) into Eq. (5) one arrives at the full antineutrino oscillation probability

$$P(\overline{\nu_e^s} \to \overline{\nu_e^d}) = \sum_{i,j} \mathcal{J}^i \mathcal{J}^{j*} - 4 \sum_{i>j} \mathrm{Re}(\mathcal{J}^i \mathcal{J}^{j*}) \sin^2\left(\frac{\Delta m_{ij}^2 L}{4E}\right) + 2 \sum_{i>j} \mathrm{Im}(\mathcal{J}^i \mathcal{J}^{j*}) \sin\left(\frac{\Delta m_{ij}^2 L}{2E}\right) , \tag{7}$$

where $\Delta m_{ij}^2 = m_i^2 - m_j^2$, and

$$\mathcal{J}^i = U_{ei} U_{ei}^* + \sum_\gamma \varepsilon_{e\gamma}^{s*} U_{\gamma i} U_{ei}^* + \sum_\gamma \varepsilon_{\gamma e}^{d*} U_{ei} U_{\gamma i}^* + \sum_{\gamma,\rho} \varepsilon_{e\gamma}^{s*} \varepsilon_{\rho e}^{d*} U_{\gamma i} U_{\rho i}^* . \tag{8}$$

In the $\varepsilon^{s,d} \to 0$ limit, Eq. (7) reduces to the standard survival probability.

In this study, the quantity of our main interest is the third term in Eq. (7) which, being linear in the sine of L/E, does not play any role in the standard oscillation case. In this respect, a potential deviation from the "standard" quadratic-sine L/E dependence in an oscillation experiment can be interpreted as a hint of non-standard antineutrino interactions, in particular if such an anomaly exhibits the characteristic linear-sine L/E shape.

D. Series expansion of the antineutrino survival probability

In practice, given the finite precision of the experimental inputs, it is very convenient to expand the survival probability (7) around the standard oscillation formula in terms of the relevant small parameters, in particular $\varepsilon^{s,d}$ which are all expected to be at most at the few per-cent level, c.f. [22] and references therein. In addition, θ_{13} is small compared to the other mixing angles (with the current CHOOZ upper limit of $\sin^2 2\theta_{13} \lesssim 0.17$) and, hence, it amounts to another useful expansion parameter. Moreover, for the Daya Bay far detector,

also the oscillation term $\Delta m_{21}^2 L/(2E)$ turns out to be at the level of 10^{-1} to 10^{-2} and, as such, it can also be viewed as a small quantity.

Taking all this into account, we obtain the following expanded form of the relevant electron antineutrino survival probability

$$
\begin{aligned}
P(\overline{\nu_e^s} \to \overline{\nu_e^d}) \simeq\ & P(\overline{\nu_e} \to \overline{\nu_e})_{\text{SM}} - 4 \Big[\text{Re} \left(\varepsilon_{e\mu}^s e^{-i\delta} + \varepsilon_{\mu e}^d e^{i\delta} \right) s_{23} s_{13} + \text{Re} \left(\varepsilon_{e\tau}^s e^{-i\delta} + \varepsilon_{\tau e}^d e^{i\delta} \right) c_{23} s_{13} \\
& +\ \text{Re} \left(\varepsilon_{e\mu}^s \varepsilon_{\mu e}^d \right) s_{23}^2 + \text{Re} \left(\varepsilon_{e\tau}^s \varepsilon_{\tau e}^d \right) c_{23}^2 + \text{Re} \left(\varepsilon_{e\mu}^s \varepsilon_{\tau e}^d + \varepsilon_{e\tau}^s \varepsilon_{\mu e}^d \right) s_{23} c_{23} \Big] \sin^2 \left(\frac{\Delta m_{32}^2 L}{4E} \right) \\
& +\ 2 \Big[\text{Im} \left(\varepsilon_{e\mu}^s e^{-i\delta} + \varepsilon_{\mu e}^d e^{i\delta} \right) s_{23} s_{13} + \text{Im} \left(\varepsilon_{e\tau}^s e^{-i\delta} + \varepsilon_{\tau e}^d e^{i\delta} \right) c_{23} s_{13} \\
& +\ \text{Im} \left(\varepsilon_{e\mu}^s \varepsilon_{\mu e}^d \right) s_{23}^2 + \text{Im} \left(\varepsilon_{e\tau}^s \varepsilon_{\tau e}^d \right) c_{23}^2 + \text{Im} \left(\varepsilon_{e\mu}^s \varepsilon_{\tau e}^d + \varepsilon_{e\tau}^s \varepsilon_{\mu e}^d \right) s_{23} c_{23} \Big] \sin \left(\frac{\Delta m_{32}^2 L}{2E} \right) \\
& +\ 2 \Big[\text{Im} \left(\varepsilon_{e\mu}^s + \varepsilon_{\mu e}^d \right) c_{12} s_{12} c_{23} - \text{Im} \left(\varepsilon_{e\tau}^s + \varepsilon_{\tau e}^d \right) c_{12} s_{12} s_{23} \Big] \left(\frac{\Delta m_{21}^2 L}{2E} \right) \qquad (9) \\
& +\ \mathcal{O} \left[\varepsilon^3, s_{13}^3, \varepsilon^2 s_{13}, \varepsilon s_{13}^2, \varepsilon s_{13} \left(\frac{\Delta m_{21}^2 L}{2E} \right), \varepsilon \left(\frac{\Delta m_{21}^2 L}{2E} \right)^2, s_{13}^2 \left(\frac{\Delta m_{21}^2 L}{2E} \right) \right],
\end{aligned}
$$

where $P(\overline{\nu_e} \to \overline{\nu_e})_{\text{SM}}$ corresponds to the standard oscillation probability, i.e., the one without NSI's which is approximately given by

$$
P(\overline{\nu_e} \to \overline{\nu_e})_{\text{SM}} \simeq 1 - 4 s_{13}^2 \sin^2 \left(\frac{\Delta m_{32}^2 L}{4E} \right) - 4 s_{12}^2 c_{12}^2 \left(\frac{\Delta m_{21}^2 L}{4E} \right)^2 + \mathcal{O} \left[s_{13}^3, s_{13}^2 \left(\frac{\Delta m_{21}^2 L}{2E} \right) \right]. \tag{10}
$$

Inspecting Eq. (9) one can recognize three qualitatively different non-standard contributions to $P(\overline{\nu_e^s} \to \overline{\nu_e^d})$: In the first two lines there is a CP-even term quadratic in sine of $\Delta m_{32}^2 L/(4E)$ which, as expected, may affect the determination of the mixing angle θ_{13}. The remaining three lines denote the CP-odd NSI effects corresponding to two different kinematical regimes characterized by Δm_{32}^2 and Δm_{21}^2, respectively. Notice that in the standard parametrization (3), the Dirac CP-violating phase groups only with the former factor. It is also worth noticing that the term proportional to Δm_{21}^2 tends to be further suppressed in the "flavor-blind" setting (with $\varepsilon_{e\mu}^{s,d} = \varepsilon_{e\tau}^{s,d}$) because of the proximity of s_{23} and c_{23}.

It shall be noted that both the standard and the NSI transition probabilities depend on the neutrino mass hierarchy. For the standard oscillations, the hierarchy-sensitive terms are of the order of $s_{13}^2 \Delta m_{21}^2 L/(2E)$ and thus can be consistently neglected in Eq. (10). The NSI-dependent terms in Eq. (9), however, contain a term linear in sine of $\Delta m_{32}^2 L/(2E)$ which, indeed, differs in sign in the normal and in the inverted hierarchy schemes, respectively. Since, however, we do not expect any distinctive NSI features to be large enough to

discriminate among these two settings (although they would certainly differ in details), in what follows, we shall deliberately stick to the normal hierarchy case, i.e., assume $\Delta m_{32}^2 > 0$.

E.   Notation and conventions

In what follows we shall adopt the following parametrization:

$$\varepsilon_{e\alpha}^s \equiv |\varepsilon_\alpha^s| \, e^{\mathrm{i}\phi_\alpha^s}, \qquad \varepsilon_{\alpha e}^d \equiv |\varepsilon_\alpha^d| \, e^{-\mathrm{i}\phi_\alpha^d}, \tag{11}$$

where the universal e index was dropped for simplicity. It is also convenient to define the source and detector phase averages Φ_α and differences $\Delta\phi_\alpha$, respectively:

$$\Phi_\alpha \equiv \tfrac{1}{2}(\phi_\alpha^d + \phi_\alpha^s), \qquad \Delta\phi_\alpha \equiv \tfrac{1}{2}(\phi_\alpha^d - \phi_\alpha^s). \tag{12}$$

The latter has a clear physical meaning: indeed, for all $\Delta\phi_\alpha \to 0$ (together with $|\varepsilon_\alpha^s| \to |\varepsilon_\alpha^d|$) one recovers a limit in which the non-standard antineutrino interactions in the detection process are of the same kind as those in the production.

III.   SPECIFIC SETTINGS

In what follows, we shall discuss two simple but phenomenologically interesting shapes of NSI's and discuss the relevant effects in the reactor antineutrino experiments.

A.   Case I: $\varepsilon_\alpha^s = \varepsilon_\alpha^{d*}$

We start with the simplest case characterized by the assumption $\varepsilon_\alpha^s = \varepsilon_\alpha^{d*} \equiv |\varepsilon_\alpha|e^{i\phi_\alpha}$ which corresponds to the situation where the production and the detection processes (including the associated non-standard interactions) are just inverse of each other. The relevant antineutrino survival probability (9) is then reduced to

$$P(\overline{\nu_e^s} \to \overline{\nu_e^d}) \simeq P(\overline{\nu_e} \to \overline{\nu_e})_{\mathrm{SM}} - 4 \left\{ s_{23}^2 |\varepsilon_\mu|^2 + c_{23}^2 |\varepsilon_\tau|^2 + 2s_{23}c_{23}|\varepsilon_\mu||\varepsilon_\tau| \cos(\phi_\mu - \phi_\tau) \right.$$
$$\left. + \; 2s_{13} \left[s_{23}|\varepsilon_\mu| \cos(\phi_\mu - \delta) + c_{23}|\varepsilon_\tau| \cos(\phi_\tau - \delta) \right] \right\} \sin^2 \left(\frac{\Delta m_{32}^2 L}{4E} \right). \tag{13}$$

Remarkably, the linear sine-dependent term in Eq. (9) vanishes and the NSI effects enter the survival probability as a mere global shift of the oscillation amplitude. This amounts to
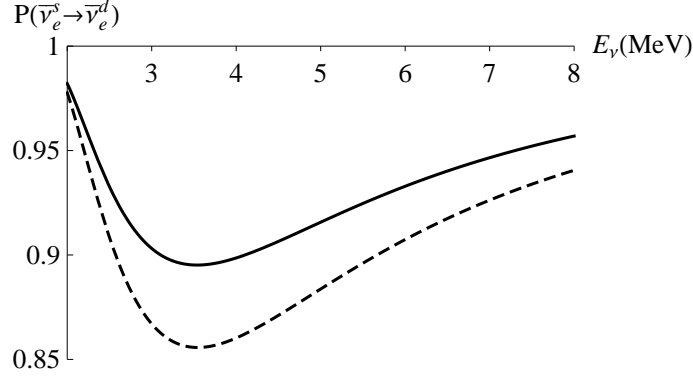
8

FIG. 1: The oscillation probability for $\sin^2 2\theta_{13} = 0.1$, $\delta = 0$ and $L = 1.8$ km with no NSI's (solid line) and with NSI's corresponding to Case I in Sect. III A with $\varepsilon_\alpha^s = \varepsilon_\alpha^{d*}$ (dashed line) where we adopted $\varepsilon_\mu = \varepsilon_\tau = 0.02$ (with both ϕ_μ and ϕ_τ fixed to zero). For the other oscillation parameters, the best-fit values have been assumed, c.f. Ref. [4].

a shift in the "effective" reactor mixing angle

$$
\begin{aligned}
s_{13}^2 \;\rightarrow\; \tilde{s}_{13}^2 \;=\; & s_{13}^2 + s_{23}^2 |\varepsilon_\mu|^2 + c_{23}^2 |\varepsilon_\tau|^2 + 2 s_{23} c_{23} |\varepsilon_\mu||\varepsilon_\tau| \cos(\phi_\mu - \phi_\tau) \\
& + \; 2 s_{13} \left[s_{23} |\varepsilon_\mu| \cos(\phi_\mu - \delta) + c_{23} |\varepsilon_\tau| \cos(\phi_\tau - \delta) \right] .
\end{aligned}
\tag{14}
$$

Namely, the oscillation probability is given by the standard formula (10) with θ_{13} replaced by the effective mixing angle $\tilde{\theta}_{13}$. Thus, there is no way to discriminate such an NSI effect from standard oscillations in reactor antineutrino experiments. It is also worth noting that the CP phase differences enter Eq. (14) via cosines only which is, indeed, justified by the CP properties of the survival probability in the setting under consideration.

In Fig. 1, we display the standard and the modified oscillation probability in the NSI presence as a function of the antineutrino energy in a detector at the "ideal" distance $L = 1.8$ km (optimized for the highest count rate at $E \sim 4$ MeV) from the source. The "depth" of the first oscillation minimum (the solid line for the standard oscillations) changes significantly if the NSI effects are turned on (dashed line); however, the energy of the minimum determined by the neutrino mass-squared differences remains essentially unchanged.[1]

---

[1] Let us remark that the energies corresponding to the two relevant minima are not exactly the same due to the presence of the sub-leading terms proportional to $\left(\Delta m_{21}^2 L/4E \right)^2$ in Eqs. (9) and (10).

Nevertheless, though the reactor antineutrino experiments in this case cannot distinguish the NSI's from a true mixing angle on their own, they can still provide a useful piece of information in combination with other types of experiments such as, e.g., accelerator experiments, superbeams, beta-beams, neutrino factories, etc. In particular, if these searches report different values of θ_{13}, NSI's could be responsible for the mismatch.

B.   Case II: $\varepsilon_\alpha^s \neq \varepsilon_\alpha^{d*}$

For $\varepsilon_\alpha^s \neq \varepsilon_\alpha^{d*}$, the production and detection processes and, in particular, the associated non-standard interactions, are not equivalent. Let us recall that in the reactor experiments the antineutrinos are produced namely by the decays of neutron-rich fission products whereas, in the detector, the antineutrinos are converted into positrons by the inverse beta decay process on the essentially free hydrogen protons. In particular, the many-body nucleon interactions during the fission processes can provide an extra contribution to the neutrino flux with no counterpart at the detection side. Though such contributions are suppressed in the SM, new physics may, at least in principle, boost these effects to an observable level.

Thus, we find it legitimate to speculate that ε^s and $\varepsilon^{d\dagger}$ might be different. As a consequence, the terms linear in sine in formula (9) are exposed and the relevant NSI effects can no longer be completely subsumed into a shift of the effective mixing angle $\tilde{\theta}_{13}$. This, besides the change of the "depth" of the first oscillation minimum (c.f. Figure 1), leads also to a shift in its energy, as illustrated in Figure 2. In particular, the dip can be shifted by as much as one MeV in both directions, depending on the specific choice of the NSI parameters.

In what follows we shall focus on two specific realizations of this setting, namely, the case when the magnitude of the NSI parameters differs between the production and detection processes (Case IIa) and the case when the relevant NSI parameters are of the same size but differ by their phases (Case IIb). Both these cases are studied numerically in Sect. IV.

1.   Case IIa: Non-standard interactions in source only

Let us exemplify the first option on a specific setting where the NSI's exhibit themselves only in the production processes, i.e., taking $\varepsilon^d = 0$. Given that, the general formula (9)
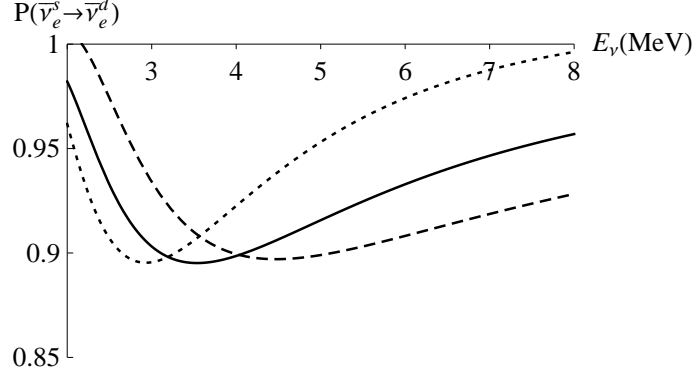
FIG. 2: The theoretical oscillation probability with no NSI (solid line) and with NSI's (dashed and dotted lines) for $L = 1.8$ km. For the sake of illustration, we adopt a flavour-universal scheme with all the relevant NSI parameters at the same level of $|\varepsilon_{\mu,\tau}| = 0.04$ with $\Delta\phi_{\mu,\tau} = \frac{\pi}{2}$. The other neutrino mixing parameters are the same as in Fig. 1. The dashed line corresponds to $\Phi_{\mu,\tau} = \frac{8}{5}\pi$ whereas the dotted one to $\Phi_{\mu,\tau} = \frac{2}{5}\pi$, respectively.

simplifies into

$$
\begin{aligned}
P(\overline{\nu_e^s} \to \overline{\nu_e^d}) \simeq\ & P(\overline{\nu_e} \to \overline{\nu_e})_{\text{SM}} \\
& - 4s_{13}\left[s_{23}|\varepsilon_\mu|\cos(\phi_\mu - \delta) + c_{23}|\varepsilon_\tau|\cos(\phi_\tau - \delta)\right]\sin^2\left(\frac{\Delta m_{32}^2 L}{4E}\right) \\
& + 2s_{13}\left[s_{23}|\varepsilon_\mu|\sin(\phi_\mu - \delta) + c_{23}|\varepsilon_\tau|\sin(\phi_\tau - \delta)\right]\sin\left(\frac{\Delta m_{32}^2 L}{2E}\right) \\
& + 2s_{12}c_{12}\left(c_{23}|\varepsilon_\mu|\sin\phi_\mu - s_{23}|\varepsilon_\tau|\sin\phi_\tau\right)\left(\frac{\Delta m_{21}^2 L}{2E}\right),
\end{aligned}
\tag{15}
$$

where we used $\varepsilon_\alpha \equiv \varepsilon_\alpha^s$ and $\phi_\alpha \equiv \phi_\alpha^s$. It is worth noting that the genuine NSI effect (due to the last two terms) is proportional to sines of differences of the Dirac CP phase δ and the CP phases of the NSI parameters ϕ_α, as expected for a CP-violating effect beyond the standard oscillation picture.

2. *Case IIb: Same-size source and detector effects with different phases:* $|\varepsilon_\alpha^s| = |\varepsilon_\alpha^d|$, $\Delta\phi_\alpha \neq 0$

An interesting complementary setting is obtained if the magnitude of the source and detector effects are assumed to be equal so that the NSI effects can only be distinguished due to the mismatch between the corresponding CP phases ϕ_α^s and ϕ_α^d. With $|\varepsilon_\alpha^s| = |\varepsilon_\alpha^d| \equiv |\varepsilon_\alpha|$,

11

the general formula (9) receives a rather symmetric form[2]

$$
\begin{aligned}
P(\overline{\nu_e^s} \to \overline{\nu_e^d}) \simeq\ & P(\overline{\nu_e} \to \overline{\nu_e})_{\text{SM}} \\
& - 4\left\{ s_{23}^2|\varepsilon_\mu|^2 \cos 2\Delta\phi_\mu + c_{23}^2|\varepsilon_\tau|^2 \cos 2\Delta\phi_\tau \right. \\
& + 2c_{23}s_{23}|\varepsilon_\mu||\varepsilon_\tau| \cos(\Delta\phi_\mu + \Delta\phi_\tau) \cos(\Phi_\mu - \Phi_\tau) \\
& + 2s_{13} \left[s_{23}|\varepsilon_\mu| \cos\Delta\phi_\mu \cos(\Phi_\mu - \delta) + c_{23}|\varepsilon_\tau| \cos\Delta\phi_\tau \cos(\Phi_\tau - \delta) \right]\Big\} \sin^2\left(\frac{\Delta m_{32}^2 L}{4E}\right) \\
& - 2\left\{ s_{23}^2|\varepsilon_\mu|^2 \sin 2\Delta\phi_\mu + c_{23}^2|\varepsilon_\tau|^2 \sin 2\Delta\phi_\tau \right. \\
& + 2c_{23}s_{23}|\varepsilon_\mu||\varepsilon_\tau| \sin(\Delta\phi_\mu + \Delta\phi_\tau) \cos(\Phi_\mu - \Phi_\tau) \\
& + 2s_{13} \left[s_{23}|\varepsilon_\mu| \sin\Delta\phi_\mu \cos(\Phi_\mu - \delta) + c_{23}|\varepsilon_\tau| \sin\Delta\phi_\tau \cos(\Phi_\tau - \delta) \right]\Big\} \sin\left(\frac{\Delta m_{32}^2 L}{2E}\right) \\
& - 4s_{12}c_{12} \left(c_{23}|\varepsilon_\mu| \sin\Delta\phi_\mu \cos\Phi_\mu - s_{23}|\varepsilon_\tau| \sin\Delta\phi_\tau \cos\Phi_\tau \right) \left(\frac{\Delta m_{21}^2 L}{2E}\right),
\end{aligned} \tag{16}
$$

where the notation specified in Eq. (12) has been used. Again, the relevant phase differences in the genuine NSI terms enter in sines. Furthermore, the formula above can be simplified to a yet more compact form

$$
\begin{aligned}
P(\overline{\nu_e^s} \to \overline{\nu_e^d}) \simeq\ & P(\overline{\nu_e} \to \overline{\nu_e})_{\text{SM}} \\
& - 4\left\{ s_{23}^2|\varepsilon_\mu|^2 \sin\left(\frac{\Delta m_{32}^2 L}{4E} + 2\Delta\phi_\mu\right) + c_{23}^2|\varepsilon_\tau|^2 \sin\left(\frac{\Delta m_{32}^2 L}{4E} + 2\Delta\phi_\tau\right) \right. \\
& + 2c_{23}s_{23}|\varepsilon_\mu||\varepsilon_\tau| \sin\left(\frac{\Delta m_{32}^2 L}{4E} + \Delta\phi_\mu + \Delta\phi_\tau\right) \cos(\Phi_\mu - \Phi_\tau) \\
& + 2s_{13}s_{23}|\varepsilon_\mu| \sin\left(\frac{\Delta m_{32}^2 L}{4E} + \Delta\phi_\mu\right) \cos(\Phi_\mu - \delta) \\
& + 2s_{13}c_{23}|\varepsilon_\tau| \sin\left(\frac{\Delta m_{32}^2 L}{4E} + \Delta\phi_\tau\right) \cos(\Phi_\tau - \delta) \Big\} \sin\left(\frac{\Delta m_{32}^2 L}{4E}\right) \\
& - 4s_{12}c_{12} \left(c_{23}|\varepsilon_\mu| \sin\Delta\phi_\mu \cos\Phi_\mu - s_{23}|\varepsilon_\tau| \sin\Delta\phi_\tau \cos\Phi_\tau \right) \left(\frac{\Delta m_{21}^2 L}{2E}\right),
\end{aligned} \tag{17}
$$

which does expose the "kinematic" role of the phase differences $\Delta\phi_\alpha$ and the "amplitude modulation" role of their averages Φ_α.

Let us also remark that for $\Delta\phi_\alpha \to 0$ (when the symmetric setting with $\varepsilon^s = \varepsilon^{d\dagger}$ is recovered) the last term vanishes and, as expected, the other terms conspire to yield a mere shift in the effective mixing angle $\tilde{\theta}_{13}$ identical to that given in formula (14). This provides

---

[2] Note that the coefficient of the last term in Eq. (16) is optically different from the same in Eq. (9) which is due to the utilized goniometric identity for a difference of two sines and the definition of $\Delta\phi_\alpha$.

a nice consistency check of the results. A simple numerical analysis of both Case-IIa and Case-IIb settings is given in Sect. IV.

IV. NON-STANDARD ANTINEUTRINO INTERACTIONS AT DAYA BAY

A. Experimental setting

The Daya Bay neutrino experiment [16] is designed to perform a precision measurement of θ_{13} using antineutrinos produced by the reactors of the Daya Bay Nuclear Power Plant (NPP) and the Ling Ao NPP. In the detectors, antineutrinos from the reactors are captured via the inverse beta-decay process, and the deficit from the expected $1/L^2$ dependence is to be interpreted as a signature of neutrino oscillations. In particular, near and far detectors are employed in order to suppress the systematic uncertainties related to the antineutrino flux from the reactors.

The Daya Bay measurement of $\sin^2 2\theta_{13}$ is expected to reach the sensitivity of the order of 0.01, an order of magnitude better than the current CHOOZ limit $\sin^2 2\theta_{13} \lesssim 0.17$. Besides a high-quality determination of the relevant standard neutrino oscillation parameters, Daya Bay can be rather efficient in improving some of the current constraints on physics beyond the SM.

In order to estimate the NSI effects possibly observable at Daya Bay, we perform a basic numerical analysis making use of a simple model of the detected neutrino spectra. There are three pairs of nuclear reactor cores of a total thermal power of 17.4 GW at the experiment site, namely, Daya Bay (DYB), Ling Ao (LA) and Ling Ao II (LAII), providing electron antineutrinos to three detectors, two near ones called Daya Bay (DYB) and Ling Ao (LA) with 40 tons and a far detector (FAR) with 80 tons of a Gadolinium-doped liquid scintillator, respectively. A more detailed breakdown of the relevant Daya Bay parameters can be found in TABLE I.

B. A simple model of the $\overline{\nu_e}$ spectra

For the sake of simplicity, we shall assume that each pair of neighboring cores constitute a single point source. The average energy release per one fission E_F is anticipated to be

Detectors / Reactors	DYB 2×2.9 GW	LA 2×2.9 GW	LAII 2×2.9 GW
DYB (40 t)	363	1347	1985
LA (40 t)	857	481	1618
FAR (80 t)	1307	526	1613

TABLE I: The basic Daya Bay experiment layout [16]: distances (in meters) between detectors (rows) and centers of pairs of the neighboring reactor cores (columns).

around 200 MeV [16] so the estimated number of fissions per second in each reactor site N_F is

$$N_F = 2\,P_T/E_f = 2 \times 2.9 \text{ GW}/200 \text{ MeV} = 1.8 \times 10^{20} \ s^{-1}\,, \tag{18}$$

where the extra factor 2 counts the number of reactor cores per site and P_T stands for the thermal power of each core. For the spectrum of the antineutrino flux per fission we shall use the approximate formula given in Ref. [24] (for E in MeV):

$$\frac{d\Phi}{dE} = \exp\left(0.87 - 0.16E - 0.091E^2\right) \text{MeV}^{-1}\,. \tag{19}$$

Antineutrinos interact with the free protons in the scintillator via the inverse beta decay process $\overline{\nu_e} + p \to n + e^+$. The cross-section of this reaction has been calculated in Ref. [25] to be

$$\sigma\left(E\right) = 9.52 \times 10^{-48} m^2 \left[\left(E - (m_n - m_p)\right)\sqrt{\left(E - (m_n - m_p)\right)^2 - m_e^2} \text{ MeV}^{-2}\right] \tag{20}$$

with the energy threshold $E_0 = 1.8$ MeV. There are 6.29×10^{22} free protons in a cm^3 of the scintillator of density $\rho = 0.86$ g/cm^3 [26]. Therefore the number of targets per one ton of the scintillator is $N_T = 7.3 \times 10^{28}$ ton^{-1}.

The antineutrino survival probability $P(\overline{\nu_e^s} \to \overline{\nu_e^d})$ is a function of energy, propagation distance, oscillation parameters and, in general, also the NSI parameters. The expected total number of antineutrino events in the detector D (with D =DYB,LA,FAR) with mass M_D after three years of running can be estimated as

$$\frac{dN_D}{dE} = t \times N_T \times M_D \times C_{eff} \times N_F \times \Phi(E) \times \sigma\left(E\right) \times \sum_{R=\text{DYB,LA,LAII}} \frac{P(\overline{\nu_e^s} \to \overline{\nu_e^d})}{4\pi L_{DR}^2}\,, \tag{21}$$

where $t = 3 \times 365 \times 24 \times 3600$ s is the duration of a three-years' run. We sum over three reactor sites and use L_{DR} for the distance between the detector D and the reactor site R,
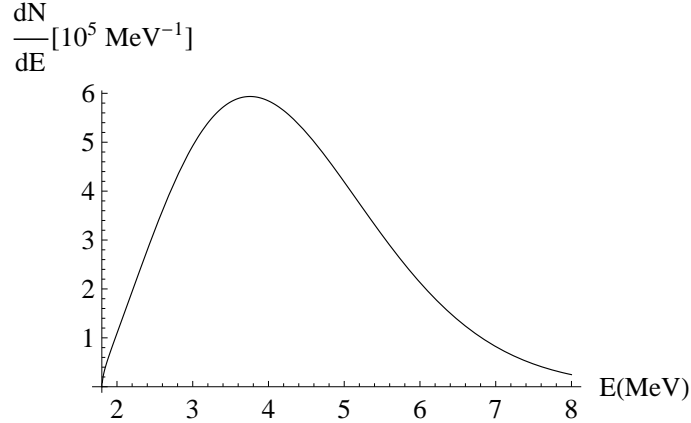
14

FIG. 3: The expected shape of the detected antineutrino spectrum in the DYB (near) detector after three years of running without NSI's.

c.f. TABLE I. In addition, we adopt a detection efficiency coefficient $C_{eff} = 0.78$ [16]. As an example, we depict in Figure 3 the expected spectrum of antineutrinos detected in the DYB detector. It is worth noting that the highest event rate corresponds to $E \simeq 4$ MeV.

The quantity of our main interest is the ratio of the antineutrino energy spectra between the considered far and near detectors, which can be obtained readily from Eq. (21). It is expected that, due to a similar design of the far and near detectors, the systematic uncertainties associated to, e.g., the absolute flux determination, can be greatly reduced in the ratio of the energy spectra. However, in order to fully account for all the systematic uncertainties, e.g., the backgrounds, energy miscalibration, detection efficiencies etc., a complex simulation of the Daya Bay experiment is necessary. This, however, is beyond the scope of this work. Thus, in what follows, we shall focus entirely on the statistical uncertainties.

C. The χ^2 analysis

To assess the observability of NSI's at Daya Bay in practice, we perform a simple numerical χ^2 analysis along the following lines: we choose 15 energy bins from 1.8 MeV to 8 MeV in order to have approximately the same statistics in all bins which are 1-4 times wider than the energy resolution $15\%/\sqrt{E(\text{MeV})}$ [16]. In each bin, we use Eq. (21) to calculate the ratio R of the antineutrino energy spectra between the far and near detectors (for sake of illustration, from now on we shall focus in particular onto the FAR and the DYB detectors). In the case of the standard neutrino oscillations, the expected shape of this ratio between
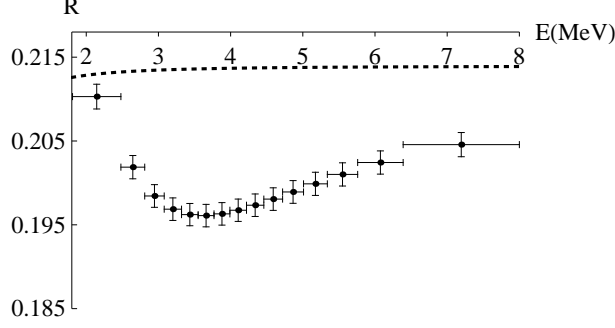
15

FIG. 4: Ratio between the FAR and the DYB detectors for standard oscillations with statistical errors only. The dotted line corresponds to the case of $\sin^2 2\theta_{13} = 0$. The neutrino mixing parameters are the same as those used in Figure 1.

the FAR and the DYB detectors is depicted in Figure 4.

Since the uncertainties of θ_{23}, θ_{12} and Δm_{21}^2 are not expected to play any significant role in the ratio of our interest, we shall fix these parameters to their central values. This is not the case of Δm_{32}^2 because the uncertainty in this parameter (quantified by $\sigma_{\Delta m_{32}^2}$) mimics the effects of the NSI's, namely, it also shifts the position of the first minimum in R. However, with the increasing precision of the Δm_{32}^2 determination, these effects become less important. Therefore, in what follows, we shall mainly focus on two specific situation corresponding to different choices of $\sigma_{\Delta m_{32}^2}$: in one case we take $\sigma_{\Delta m_{32}^2} = 0.09 \times 10^{-3} \mathrm{eV}^2$ [4] as the current experimental value while in the other "ideal case", we push $\sigma_{\Delta m_{32}^2}$ down to $0.025 \times 10^{-3} \mathrm{eV}^2$, respectively (which can be viewed as an optimistic expectation for the uncertainty in the atmospheric mass-squared difference in several years from now).

For each specific choice of the relevant NSI parameters there are only two unknown parameters left in R, namely, $s_{13} \equiv \sin \theta_{13}$ and Δm_{32}^2, c.f., Eq. (10). Denoting the i-th bin value of R (as a function of s_{13}, Δm_{32}^2, ε^s and ε^d) by $R_i(s_{13}, \Delta m_{32}^2, \varepsilon^s, \varepsilon^d)$, we attempt to fit the simulated data by the NSI null-hypothesis corresponding to the case when R_i is calculated for standard oscillations with some effective values of the relevant oscillation parameters, namely, $R_i^0 (\tilde{s}_{13}, \Delta \tilde{m}_{32}^2)$. This is done by minimization of the χ^2 function

$$\chi^2 = \sum_{i=1}^{15} \left[\frac{R_i \left(s_{13}, \Delta m_{32}^2, \varepsilon^s, \varepsilon^d \right) - R_i^0 \left(\tilde{s}_{13}, \Delta \tilde{m}_{32}^2 \right)}{\sigma_{\mathrm{data}}} \right]^2 + \left(\frac{\Delta m_{32}^2 - \Delta \tilde{m}_{32}^2}{\sigma_{\Delta m_{32}^2}} \right)^2 \quad (22)$$

with respect to $\tilde{s}_{13}$ and $\Delta \tilde{m}_{32}^2$, where σ_{data} denotes the three-years' run statistical error(s). The $\tilde{s}_{13}$ parameter has been left free (to be determined by Daya Bay) whereas $\Delta \tilde{m}_{32}^2$ should

obey the existing experimental constraints. The value of χ^2 in the minimum $(\chi^2_{\min})$ then quantifies the likelihood that the Daya Bay data could be fitted by the standard oscillation formula. For two fitted parameters, $\chi^2_{\min} = 2.3$ and 4.61 corresponds to 68% and 90% C.L., respectively.

D.   Results

For the sake of simplicity, in what follows we shall consider only the "flavorless" versions of the oscillation probability formulas relevant to the three cases of our interest, namely Eqs. (13), (15) and (17). This amounts to setting $\phi_\mu = \phi_\tau \equiv \phi$ and $|\varepsilon_\mu| = |\varepsilon_\tau| \equiv |\varepsilon|$ everywhere. Let us recall that, besides the standard oscillation parameters, in Case I and Case IIa the relevant input NSI parameters are, namely, the (universal) magnitude of the NSI effects $|\varepsilon|$ and the corresponding CP phase ϕ (more precisely, the phase difference $\phi' = \phi - \delta$ where δ denotes the leptonic Dirac CP phase) while in Case IIb the NSI parameters entering the survival probability are $|\varepsilon|$, Φ (again, it is rather $\Phi' = \Phi - \delta$) and $\Delta\phi$.

Let us also reiterate that only the statistical errors have been taken into account in the current analysis. A complete study including also the systematic uncertainties would require a complex simulation of the Daya Bay experiment. This, however, is beyond the scope of the present study.

1.   Case I

As we argued in Sect. III A, in the symmetric setting with $\varepsilon^s = \varepsilon^{d\dagger}$, the NSI effects cannot be distinguished from the pure standard oscillations. Even if the underlying mixing angle θ_{13} is zero, one can still fit the data with a standard oscillation curve corresponding to a nonzero value of the effective mixing angle $\tilde{\theta}_{13}$ given by formula (14). A pair of representative plots depicting the expected ratio between the FAR and the DYB antineutrino spectra in this situation are given in Figure 5. One can see that the data are well fitted by the standard oscillation formula with just the effective mixing angles different from their "true" values.
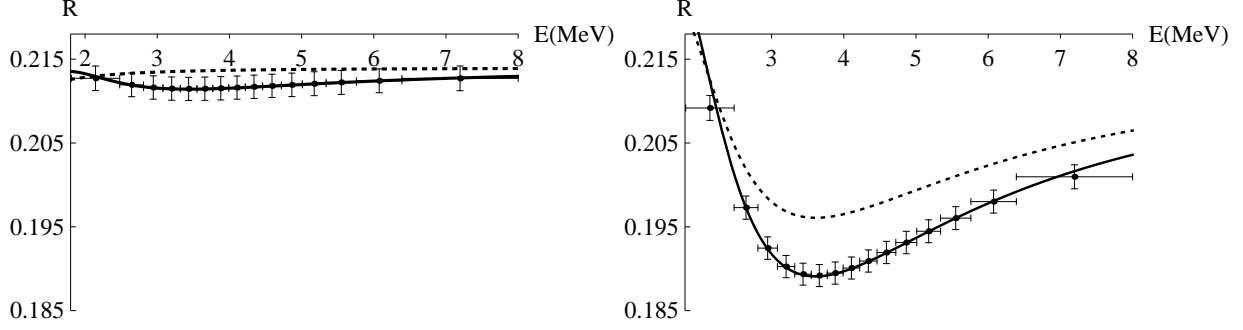
17

FIG. 5: Sample fits of the ratio between the detected antineutrino spectra in the FAR and DYB near detectors in the case that the production and detection process (including the relevant non-standard interactions) are just inverse of each other (Case I, Sect. III A), i.e., $\varepsilon^s = \varepsilon^{d\dagger}$. In the left panel, $\sin^2 2\theta_{13} = 0$, $|\varepsilon| = 0.04$ and $\phi' = 0$ have been used; in the right panel, $\sin^2 2\theta_{13} = 0.1$, $|\varepsilon| = 0.02$ and $\phi' = 0$ instead. The dotted lines correspond to the standard oscillations without NSI's, while the solid lines are the fits based on the standard oscillation survival probability (10) used in Eq. (21) with the effective mixing angles given by $\sin^2 2\tilde{\theta}_{13} = 0.013$ (left panel) and $\sin^2 2\tilde{\theta}_{13} = 0.138$ (right panel).

2. Case IIa

In the "flavorless" setting, the relevant Case-IIa formula (15) simplifies into

$$
\begin{aligned}
P(\bar{\nu}_e^s \to \bar{\nu}_e^d) \simeq\ & P(\bar{\nu}_e \to \bar{\nu}_e)_{\mathrm{SM}} - 4s_{13}(s_{23} + c_{23})|\varepsilon|\cos\phi'\sin^2\left(\frac{\Delta m_{32}^2 L}{4E}\right) \\
& + 2s_{13}(s_{23} + c_{23})|\varepsilon|\sin\phi'\sin\left(\frac{\Delta m_{32}^2 L}{2E}\right) \\
& + 2s_{12}c_{12}(c_{23} - s_{23})|\varepsilon|\sin\phi\left(\frac{\Delta m_{21}^2 L}{2E}\right),
\end{aligned}
\tag{23}
$$

where $\phi' \equiv \phi - \delta$. Note that in most cases the last term can be neglected due to the experimental proximity of θ_{23} to $\frac{\pi}{4}$.

We also stress that for $\phi' \to 0$ or π the leading NSI contribution corresponding to the sine-squared term above essentially mimics the effects of standard oscillations with a shifted mixing angle because, besides the last negligible term, there is no net NSI induced CP-violating effect. One can see this on the left panel in Figure 6 where, indeed, the data can be fitted by the standard oscillation formula with just a shifted effective mixing angle $\tilde{\theta}_{13}$. However, the change is still proportional to s_{13} and thus no shift is induced if the underlying
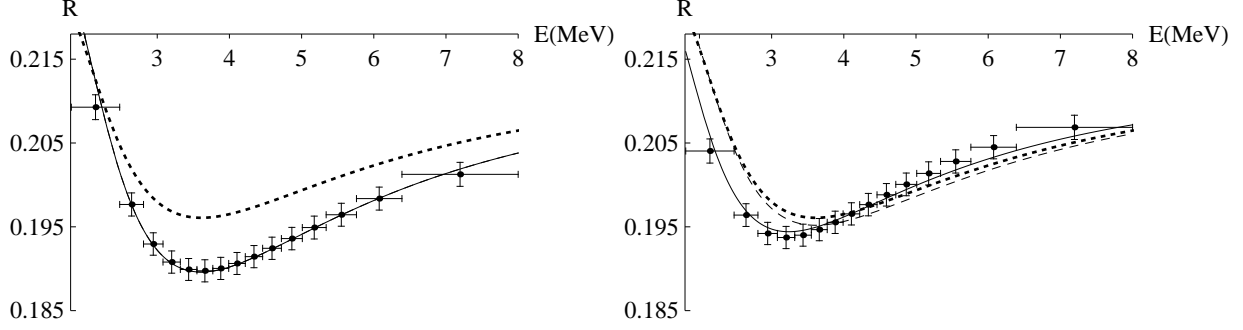
18

FIG. 6: Sample fits of the ratio between the detected antineutrino spectra in the FAR and DYB near detectors in the asymmetric setting where the NSI's are assumed to affect only the production process (Case IIa, Sect. III B 1). We adopt $\sin^2 2\theta_{13} = 0.1$ and $|\varepsilon| = 0.04$ in both panels. Furthermore, in the left panel, $\phi' = 0$ is assumed, while in the right panel we take $\phi' = \frac{\pi}{2}$ (maximal CP phase difference). The dotted lines correspond to the standard oscillations without NSI's, while the dashed lines show the fitted curves with the effective mixing angle $\sin^2 2\tilde{\theta}_{13} = 0.135$ (left panel) and $\sin^2 2\tilde{\theta}_{13} = 0.105$ (right panel). In addition, the solid lines stand for the fitted curves with two parameters $\tilde{\theta}_{13}$ and $\Delta\tilde{m}_{32}^2$. In the left panel, the solid line coincides with the dashed line, whereas in the right panel it does not and the best fit corresponding to the values $\sin^2 2\tilde{\theta}_{13} = 0.109$ and $\Delta\tilde{m}_{32}^2 = 2.20 \times 10^{-3}$ eV^2 requires a significant shift in $\Delta\tilde{m}_{32}^2$ with rescpect to its central value.

θ_{13} happens to be zero[3].

However, for non-trivial ϕ', the NSI effects can no longer be subsumed into a pure shift in θ_{13} and the standard oscillation formula no longer fits the data even if one admits for a certain variation in Δm_{32}^2, see the right panel in Figure 6. Thus, in this case, one can in principle attempt to constrain the $|\varepsilon|$ and ϕ' parameters, at least in some parts of their parameter space.

In Figure 7 we present the relevant exclusion regions for these parameters. Therein, one can observe an intersting π-periodicity in ϕ', which can be understood from the shape of the second correction in formula (23). Remarkably enough, even with variable Δm_{32}^2 and $|\varepsilon|$ as low as 0.02, in some cases the NSI effects can be distinguished from the standard oscillation at 90% C.L.

---

[3] As we shall see, this is different from the Case IIb setting studied in Sect. IV D 3 where a nonzero value of the effective mixing angle can be generated even for $\theta_{13} = 0$.
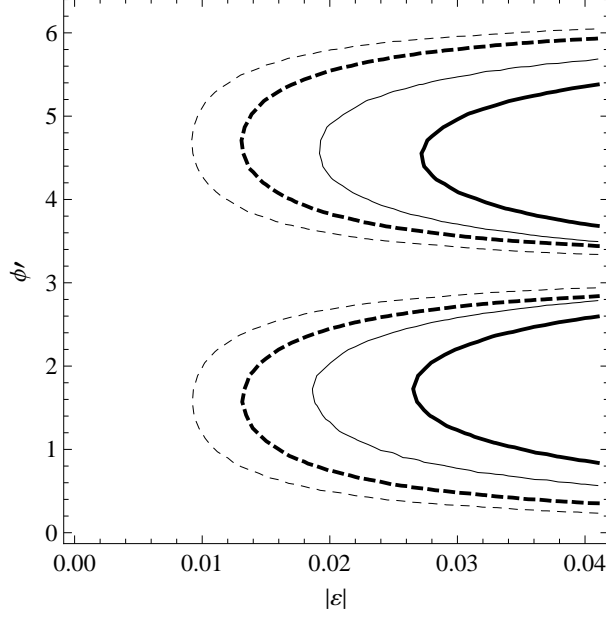
FIG. 7: Regions of parameters (on the right hand side of the curves), where the Daya Bay experiment can disfavour the standard oscillation hypothesis at 68% (thin curves) and at 90% (thick curves) C.L. for $\sin^2 2\theta_{13} = 0.1$. The solid curves stand for a standard two-parameter fit with variable θ_{13} and Δm_{32}^2 while the dashed curves correspond to the fit with $\sigma_{\Delta m_{32}^2}$ pushed down to $0.025 \times 10^{-3} \text{eV}^2$.

3. Case IIb

In the more general case when both the source and detector effects are present there is an extra set of parameters at play associated to ε_α^d, i.e., the relevant magnitudes $|\varepsilon_\alpha^d|$ and also the extra detector NSI phases ϕ_α^d which combine with the source ones into the phase averages Φ_α and the phase differences $\Delta\phi_\alpha$, c.f. Eq. (12). As before, we will assume a "flavorless" form of NSI's and deliberately put $|\varepsilon^d| = |\varepsilon^s| \equiv |\varepsilon|$ in order to simplify the numerical analysis. Then formula (16) reduces to

$$
\begin{aligned}
P(\bar{\nu}_e^s \to \bar{\nu}_e^d) \simeq{}& P(\bar{\nu}_e \to \bar{\nu}_e)_{\text{SM}} \\
& - 4(s_{23}+c_{23})^2|\varepsilon|^2 \sin\left(\frac{\Delta m_{32}^2 L}{4E}\right) \sin\left(\frac{\Delta m_{32}^2 L}{4E} + 2\Delta\phi\right) \\
& - 8s_{13}(s_{23}+c_{23})|\varepsilon| \cos\Phi' \sin\left(\frac{\Delta m_{32}^2 L}{4E}\right) \sin\left(\frac{\Delta m_{32}^2 L}{4E} + \Delta\phi\right) \\
& - 4s_{12}c_{12}(c_{23}-s_{23})|\varepsilon| \sin\Delta\phi \cos\Phi\left(\frac{\Delta m_{21}^2 L}{2E}\right),
\end{aligned}
\tag{24}
$$

where, again, $\Phi' \equiv \Phi - \delta$. As before, the last term is negligible for θ_{23} close to $\pi/4$.
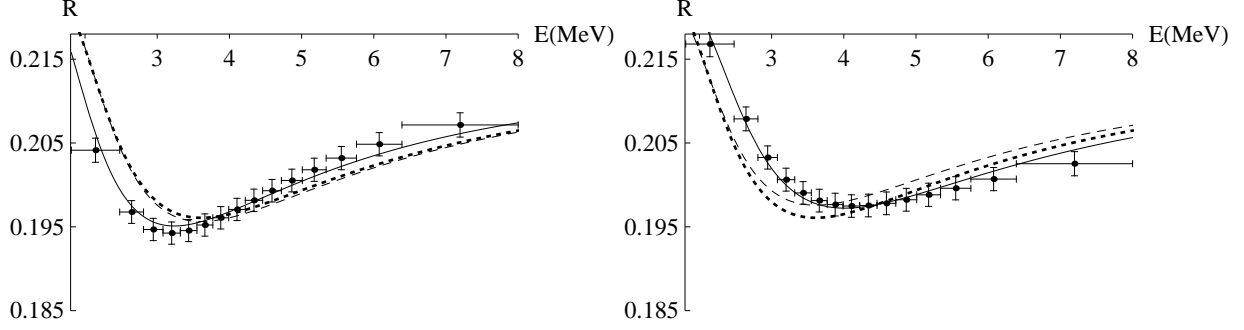
FIG. 8: Sample fits of the ratio between the detected antineutrino spectra in the FAR and DYB near detectors in Case IIb. We adopt $\sin^2 2\theta_{13} = 0.1$ and $|\varepsilon| = 0.02$ as well as $\Delta\phi = \frac{\pi}{2}$ in both panels. Furthermore, in the left panel, $\Phi' = \frac{\pi}{2}$ is assumed, while in the right panel we put $\Phi' = \frac{3}{2}\pi$. The dotted lines correspond to the standard oscillations without NSI's, while the dashed lines show the fitted curves with the effective mixing angle $\sin^2 2\tilde{\theta}_{13} = 0.103$ (left panel) and $\sin^2 2\tilde{\theta}_{13} = 0.092$ (right panel). In addition, the solid lines stand for the fitted curves with two parameters, i.e., $\sin^2 2\tilde{\theta}_{13} = 0.105$ and $\Delta\tilde{m}_{32}^2 = 2.20 \times 10^{-3}$ eV^2 in the left panel, and $\sin^2 2\tilde{\theta}_{13} = 0.094$ and $\Delta\tilde{m}_{32}^2 = 2.72 \times 10^{-3}$ eV^2 in the right panel.

For the sake of illustration, in Figure 8 we show two specific examples of the R-fits obtained in Case IIb. There, the data are fitted by the standard oscillations, first with variable θ_{13} and Δm_{32}^2 (solid lines) and then also with only θ_{13} as a free parameter (dashed lines).

In Figure 9, the exclusion plots for the $\Delta\phi$ and $|\varepsilon|$ parameters are given for $\sin^2 2\theta_{13}$ and two specific choices of Φ'. The sensitivity in $|\varepsilon|$ is similar to that observed in Figure 8 for Case IIa. Notice, however, that the two leading corrections in Eq. (16) have a very different $\Delta\phi$-periodicity. The former is π-periodic in $\Delta\phi$ while the latter is $\frac{\pi}{2}$-periodic in $\Delta\phi$. The reason is easily seen from the analytic shape of the relevant survival probability (24). Indeed, for $\Phi' = 0$, the second correction in formula (24) dominates over the first one while it is the other way round for $\Phi' = \frac{\pi}{2}$.

Regions in the $\Phi' - \Delta\phi$ plane where Daya Bay experiment could distinguish non-standard effects from standard oscillations (at 68% and 90% C.L.) are shown in Figure 10 for different values of $|\varepsilon|$ and $\sin^2 2\theta_{13}$. If the value of the underlying θ_{13} is close to the CHOOZ limit ($\sin^2 2\theta_{13} < 0.17$) and $|\varepsilon| = 0.02$ then the region is relatively large, see the upper-left panel in Figure 10. With decreasing $|\varepsilon|$ (from left to right) or θ_{13} (from up to down), the observability
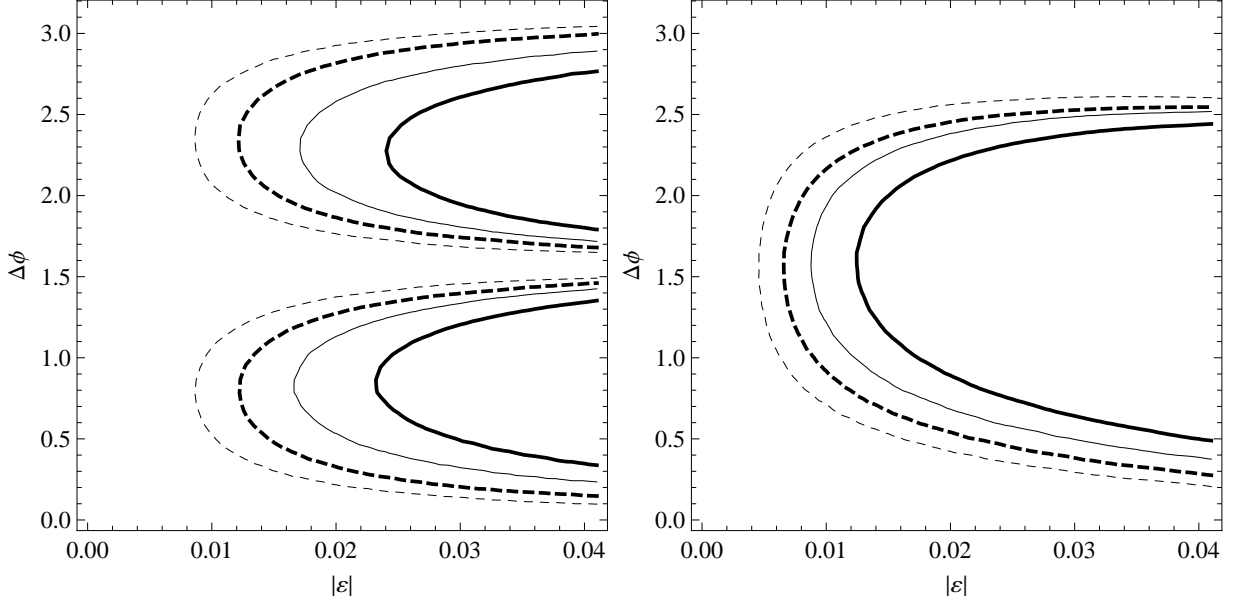
FIG. 9: Regions of parameters (on the right hand side of the curves), where the Daya Bay experiment can disfavour the standard oscillation hypothesis at 68% (thin curves) and at 90% (thick curves) C.L. for $\sin^2 2\theta_{13} = 0.1$ and $\Phi' = 0$. Here we assume $\Phi' = 0$ (left panel) and $\Phi' = \frac{\pi}{2}$ (right panel). As before, the solid curves stand for a standard two-parameter fit with variable θ_{13} and Δm_{32}^2 while the dashed curves correspond to the fit with $\sigma_{\Delta m_{32}^2}$ pushed down to $0.025 \times 10^{-3} \mathrm{eV}^2$.

domains become naturally smaller.

The possible NSI effects in an independent Daya Bay determination of the standard oscillation parameters θ_{13} and Δm_{32}^2 are illustrated in Figure 11. One can see that, at least in some cases, the corresponding global best fit point can differ significantly from the "true" values of these parameters, potentially leading to a tension between Daya Bay and other experiments.

Yet another comment is in order here. As we have seen in Case IIa (c.f., Sect. IV D 2), with source effects only there is no way to end up with a significant effective θ_{13} if the underlying θ_{13} was zero, while here one still gets $\tilde{\theta}_{13} \neq 0$ even for $\theta_{13} = 0$ due to the first term in Eq. (24). Such a qualitative difference in the behavior of these two settings can be heuristically understood as follows: In the former case, there are effectively only two small parameters (with their corresponding CP phases) at play, namely $|\varepsilon^d|$ and s_{13} while there are three such quantities in the latter case, in particular $|\varepsilon^s|$, $|\varepsilon^d|$ and s_{13}. In Case IIa, there is thus only a single relevant phase difference governing the CP-even effects [due to
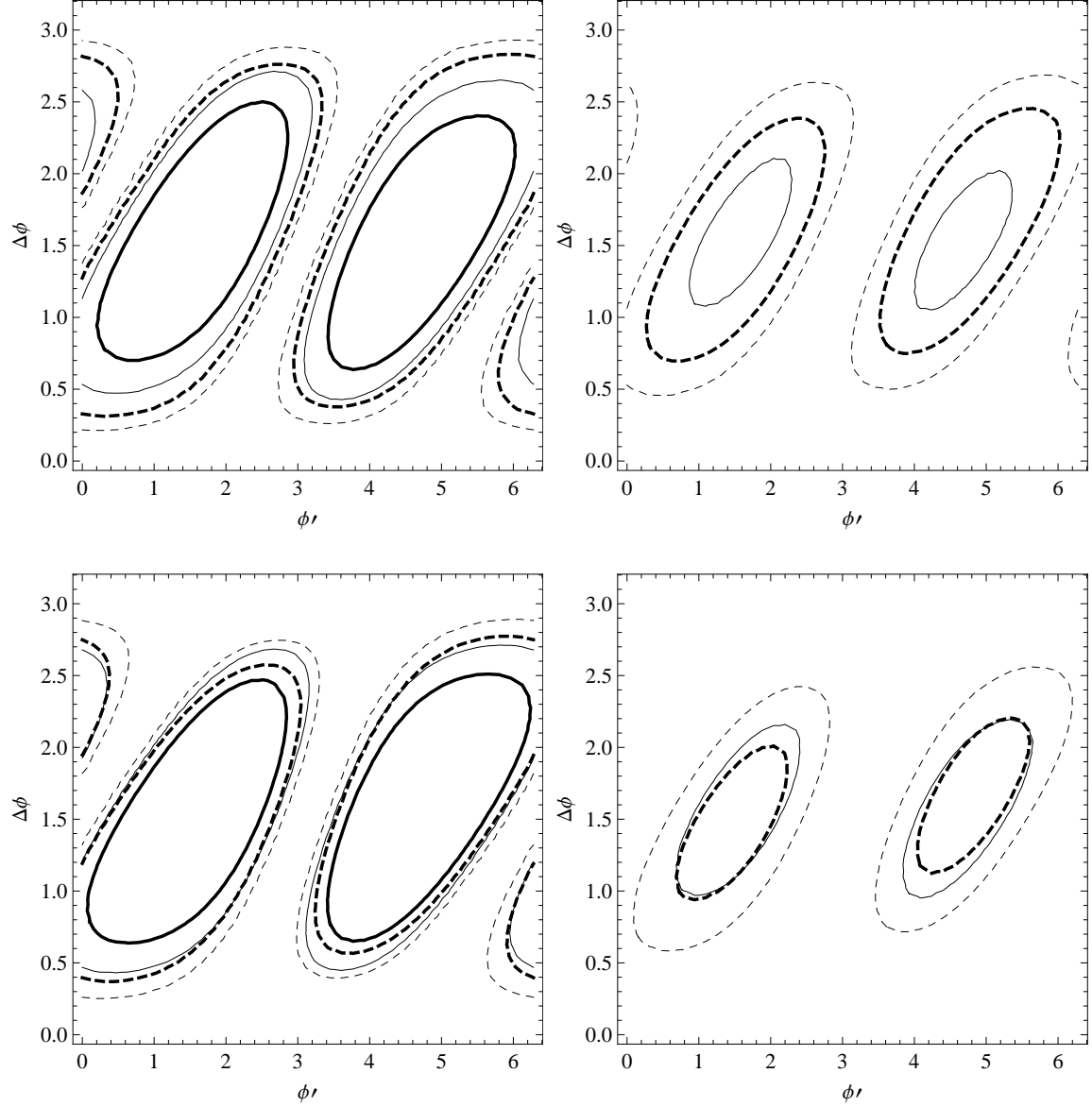
22

FIG. 10: Regions of parameters (interior), where the Daya Bay experiment can disfavour the standard oscillation hypothesis at 68% (thin curves) and at 90% (thick curves) C.L. for $|\varepsilon| = 0.02$ (left column) and $|\varepsilon| = 0.01$ (right column) and $\sin^2 2\theta_{13} = 0.1$ (upper row) and $\sin^2 2\theta_{13} = 0.05$ (lower row). Again, the solid curves stand for a standard two-parameter fit with variable θ_{13} and Δm_{32}^2 while the dashed curves correspond to the fit with $\sigma_{\Delta m_{32}^2}$ pushed down to $0.025 \times 10^{-3} \text{eV}^2$.

the first correction in Eq. (23)] which, however, becomes ill defined in the $s_{13} \to 0$ limit, and thus its effect can be "rotated away". Remarkably, this is not so in Case IIb since there is an observable phase difference $\Delta\phi$ left even in the $s_{13} \to 0$ limit and the corresponding contribution to the effective $\tilde{\theta}_{13}$ due to the first term in Eq. (24) cannot be transformed out.
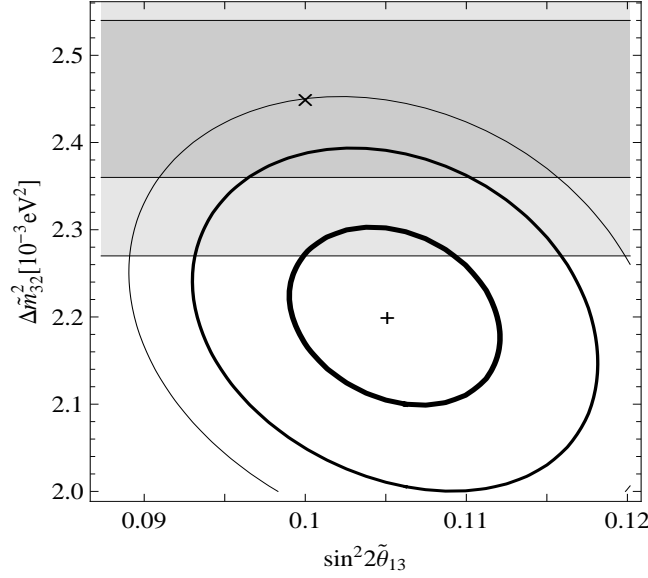
FIG. 11: The effects of the non-standard interactions in the determination of the standard oscillation parameters θ_{13} and Δm^2_{32} at Daya Bay after 3 years of running. The upper cross denotes the assumed "true" values of the standard oscillation parameters $\sin^2 2\theta_{13} = 0.1$, $\Delta m^2_{32} = 2.45 \times 10^{-3}\text{eV}^2$. Turning on the NSI parameters (fixing, for instance, $|\varepsilon| = 0.02$, $\Phi = \pi/2$, $\Delta\phi = \pi/2$ in case IIb, c.f., Sect. III B 2), the best standard oscillation fit is shifted to $\sin^2 2\tilde\theta_{13} = 0.105$ and $\Delta \tilde m^2_{32} = 2.20 \times 10^{-3}\text{eV}^2$ (the lower cross) and the corresponding $\chi^2_{\min} = 12.6$ indicates a significant incompatibility between the Daya Bay data and the standard oscillation hypothesis. We display three solid curves depicting the χ^2 levels around the best-fit point; from thick to thin, $\chi^2 = 20, 40$ and 60, respectively. The shaded bands depict the pull (due to the second term in Eq. (22)) inflicted by $\Delta \tilde m^2_{32}$ departing from the "true value"; the dark/light and light/white boundaries enclose the $\Delta \tilde m^2_{32} = (2.45 \pm 0.09) \times 10^{-3}\text{eV}^2$ and $\Delta \tilde m^2_{32} = (2.45 \pm 0.18) \times 10^{-3}\text{eV}^2$ regions (about 1σ and 2σ), respectively.

V. SUMMARY AND OUTLOOK

In this work, we have performed a detailed analysis of the non-standard antineutrino interaction effects in the Daya Bay short-baseline reactor antineutrino experiment.

The NSI's in reactor antineutrino experiments can exhibit themselves in various ways depending on the character of the underlying physics. If, for instance, the non-standard interactions in the production and detection processes happen to be exactly the same, i.e.,

$\varepsilon^s = \varepsilon^{d\dagger}$, the net effect consists in a shift in the depth of the oscillation dip in the measured ratio of the far and near detector antineutrino spectra corresponding to the extracted value of the mixing angle θ_{13}. Thus, in this case, the NSI effects can not be distinguished from the standard oscillations [20].

If, however, this assumption is relaxed, owing to, e.g., non-standard multi-body interactions in the source, the measured antineutrino spectra are distorted in a specific way and become incompatible with the standard oscillation interpretation – besides the change of the depth of the first dip, also its energy position is shifted. This can be only partially accounted for by the standard oscillation formula if the extracted values of the mixing angle θ_{13} and, in particular, the corresponding mass-squared difference Δm_{32}^2, are both allowed to differ significantly from their genuine values. However, in practice, the effect can not be entirely subsumed into a shift in the $\theta_{13} - \Delta m_{32}^2$ plane due to the strict constraints on these parameters from other measurements.

In Sect. II, we have derived general formulas for the oscillation probabilities including the non-standard effects in the antineutrino production and detection processes, arguing that the matter effects throughout the antineutrino propagation do not play any significant role in short baseline reactor neutrino experiments such as Daya Bay.

In Sect. III we specified the setting of our main interest corresponding to three different configurations of the NSI parameters. In Sect. IV we performed an illustrative numerical analysis of these settings based on an empirical model of the reactor antineutrino spectrum at Daya Bay assuming for simplicity that the NSI effects are flavour blind. Taking into account the statistical uncertainties corresponding to three years of running, we have studied how the NSI's could modify the antineutrino energy spectra and the measured values of the neutrino mixing parameters in practice. We observe that, under certain conditions, the Daya Bay experiment can provide hints of such non-standard effects at more than 90% C.L.

We should also stress the important complementary role the long baseline experiments, such as, e.g., accelerator experiments, superbeams, beta-beams or a neutrino factory, could play. Namely, if θ_{13} or Δm_{32}^2 as determined by Daya Bay differ significantly from the other results, one would have to take the NSI effects seriously as one of the possible sources of such a discrepancy. In that case, a combined analysis of the Daya Bay data together with the data from the other experiments, including the NSI's of the kind considered in this study, would be of utmost importance.

Acknowledgments

---

[1] MINOS collaboration, P. Adamson *et al.*, Phys.Rev.Lett. (2011), arXiv:1104.0344.

[2] MiniBooNE collaboration, A. A. Aguilar-Arevalo *et al.*, Phys. Rev. Lett. **105**, 181801 (2010), arXiv:1007.1150.

[3] LSND, A. Aguilar *et al.*, Phys. Rev. **D64**, 112007 (2001), arXiv:hep-ex/0104049.

[4] T. Schwetz, M. Tortola, and J. Valle, (2011), arXiv:1103.0734.

[5] R. Foot, H. Lew, X. G. He, and G. C. Joshi, Z. Phys. **C44**, 441 (1989).

[6] M. Gell-Mann, P. Ramond, and R. Slansky, Complex spinors and unified theories, in *Supergravity*, edited by P. van Nieuwenhuizen and D. Freedman, p. 315, 1979.

[7] G. Lazarides, Q. Shafi, and C. Wetterich, Nucl. Phys. **B181**, 287 (1981).

[8] P. Minkowski, Phys. Lett. **B67**, 421 (1977).

[9] R. N. Mohapatra and G. Senjanović, Phys. Rev. Lett. **44**, 912 (1980).

[10] R. N. Mohapatra and G. Senjanovic, Phys. Rev. **D23**, 165 (1981).

[11] J. Schechter and J. W. F. Valle, Phys. Rev. **D22**, 2227 (1980).

[12] T. Yanagida, Horizontal gauge symmetry and masses of neutrinos, in *Proc. Workshop on the Baryon Number of the Universe and Unified Theories*, edited by O. Sawada and A. Sugamoto, p. 95, 1979.

[13] T. Han and B. Zhang, Phys. Rev. Lett. **97**, 171804 (2006), arXiv:hep-ph/0604064.

[14] F. del Aguila and J. A. Aguilar-Saavedra, Nucl. Phys. **B813**, 22 (2009), arXiv:0808.2468.

[15] CHOOZ, M. Apollonio *et al.*, Eur. Phys. J. **C27**, 331 (2003), arXiv:hep-ex/0301017.

[16] Daya-Bay, X. Guo *et al.*, (2007), arXiv:hep-ex/0701029.

[17] Double Chooz, F. Ardellier *et al.*, (2006), arXiv:hep-ex/0606025.

[18] RENO Collaboration, S.-B. Kim, Prog.Part.Nucl.Phys. **64**, 346 (2010).

[19] J. Kopp, M. Lindner, T. Ota, and J. Sato, Phys. Rev. **D77**, 013007 (2008), arXiv:0708.0152.

[20] T. Ohlsson and H. Zhang, Phys. Lett. **B671**, 99 (2009), arXiv:0809.4835.

[21] P. Huber, T. Schwetz, and J. W. F. Valle, Phys. Rev. **D66**, 013006 (2002), arXiv:hep-ph/0202048.

[22] C. Biggio, M. Blennow, and E. Fernandez-Martinez, JHEP **08**, 090 (2009), arXiv:0907.0097.

[23] Particle Data Group, C. Amsler *et al.*, Phys. Lett. **B667**, 1 (2008).

[24] P. Vogel and J. Engel, Phys.Rev. **D39**, 3378 (1989).

[25] P. Vogel and J. F. Beacom, Phys.Rev. **D60**, 053003 (1999), arXiv:hep-ph/9903554.

[26] I. Nemchenok, Liquid scintillator on the base of the linear alkybenzene, Daya Bay internal report.